Solar Energy 269 (2024) 112343

Contents lists available at ScienceDirect

Solar Energy

journal homepage: www.elsevier.com/locate/solener

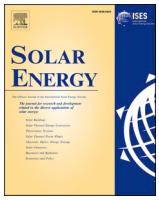

Research on temperature anomalies caused by the shading of individual solar cells in photovoltaic modules

Yang Hong [a], Ming Zhu [b], Kangwen Sun [a,*], Jian Gao [a], Chuan Shan [a]

[a] School of Aeronautic Science and Engineering, China
[b] Institute of Unmanned System, China

ARTICLE INFO

Keywords:
Shaded solar cell
Temperature
Reverse bias
Multi-physics simulation
Power

ABSTRACT

The photovoltaic industry has flourished with the increasing importance of the new energy industry. However, partial shading can cause a decrease in the output power and abnormal temperature rise of photovoltaic module. Currently, there is little research and explanation on the mechanism of the impact of shading on temperature and output power of individual solar cells in photovoltaic modules. This study investigates the temperature and power variations resulting from shading on individual solar cells at different ranges within series-connected photovoltaic modules through experiments and simulation models. Based on the experimental and simulation results, it was found that small-area shading has minimal impact on the temperature and power of photovoltaic modules. However, a sudden change in temperature and power occurs at 25% shading due to current mismatch and reverse bias voltage in the solar cells. The temperature reaches its maximum value at 40% shading, but starts to decrease when the shading range exceeds 60%, attributed to a decrease in Joule heat generated by the shaded cells. Eventually, the shaded cell acts as a high-resistance resistor in the circuit, hindering the flow of current. This study provides valuable insights into the shading effects on series-connected solar cells with an external constant current load, which can be useful for related research in this field.

1. Introduction

In recent years, with the increased emphasis on environmental protection in human society, solar energy have been increasingly used as a green and clean energy source in various fields [3]. In order to meet voltage requirements, multiple solar cells are often connected in series to form a module. The module operates at its optimal state when the series cells have matched electrical properties [1,16]. However, special attention needs to be paid to the current mismatch caused by shading, as the reverse bias caused by shading has adverse effects on the entire module [23,25].

In practical use, external factors such as vegetation, fallen leaves, snow, clouds, stains, dust, etc. [19] can shade the sunlight that falls on solar cells. The shaded cells generate a current that is smaller than their normal operating current [31], causing the other series-connected unshaded cells to provide reverse bias voltage to the shaded cells [7]. This is because the photocurrent from the unshaded cells flows through the shaded cells, leading to power dissipation and abnormal increase in the temperature of the cell [29]. The localized heating caused by partial shading can potentially raise the cell temperature above the upper limit of the packaging material, resulting in detrimental effects on the solar cell encapsulation structure and even irreversible damage to the cell itself [14]. Therefore, understanding the operating characteristics of solar cells under different shading conditions and the changes in current and voltage in their respective modules is crucial for evaluating the electrical and thermal performance, estimating the service life and developing the maintenance schedule of the solar arrays in their applications.

Over the past few years, research on shading in solar photovoltaic modules mainly focuses on changes in the output characteristics of the modules [2,9],power losses [17,20], abnormal temperature distribution patterns [30], and improvements in bypass diodes [21]. Magdaleno et al. [18] conducted a comprehensive analysis on partial shading of solar cell. They designed a shading scenario to represent real-life shading situations, where shadows covered multiple cells in different bypass diode protection segments, resulting in a significant decrease in array power output. In the worst-case scenario, this shading scenario caused power losses of up to 70 %. Sharma et al. [26] conducted shade

* Corresponding author.
E-mail addresses: hongyang2105@buaa.edu.cn (Y. Hong), Zhuming@buaa.edu.cn (M. Zhu), sunkw100@buaa.edu.cn (K. Sun), gaojian_513@163.com (J. Gao), shanchuan@buaa.edu.cn (C. Shan).

https://doi.org/10.1016/j.solener.2024.112343
Received 23 August 2023; Received in revised form 28 December 2023; Accepted 11 January 2024
Available online 30 January 2024

testing experiments on three types of solar cell modules: monocrystalline, polycrystalline, and heterojunction intrinsic thin-layer (HIT) cells. The study showed that if solar cells are partially shaded, they can experience reverse bias destruction. A large number of cells in a module can provide the driving force for reverse breakdown, resulting in high temperatures, high current density, and high encapsulation materials, which ultimately reduce the performance of the solar module. [13] conducted thermal modeling of photovoltaic cells. Under shading conditions, the cells may undergo a rapid temperature rise process (referred to as the hotspot phenomenon), which reduces the provided power. The conclusions drawn from this model were unexpected, as partially shaded photovoltaic cells entered the hotspot environment faster than fully shaded cells, providing useful insights for photovoltaic array design. For instance, an array composed of smaller cells may outperform an array composed of larger cells.

In a separate study, Clement et al. [4] conducted shade testing experiments on tiled solar cells, where the cells were subjected to shading under constant current and short-circuit operating modes. Temperature measurements of the cells under different shading areas were carried out using thermal imaging. As the shading area increased, the temperature of the cells gradually rose. At 60 % shading area, the temperature reached a maximum of 145℃. However, with further increase in shading area, the temperature gradually decreased.

Currently, most of the research on shading in solar cells tends to focus on partial shading of the entire solar cell module, with the main emphasis on overall power loss and high-temperature conditions. There is, however, a lack of research on the reverse bias voltage and temperature rise characteristics of individual solar cells under shading conditions.

Vumbugwa et al. [28] conducted a study on the shading of individual cells in photovoltaic modules. The study suggests that under constant current load conditions, the shaded cells can still generate some output when biased with forward voltage. When biased with reverse voltage, they consume energy and their temperature increases. The mismatch of operating points for individual cells will affect the overall current and voltage delivered by the module, thereby impacting the maximum power point of the module. Nevertheless, this study did not further explain the patterns and causes of abnormal temperature in single shaded cells.

Under shading conditions, the dissipated power of the cell primarily depends on the reverse I-V characteristics of the individual cell. In a reverse bias state, even small currents may require a significant reverse voltage, and high temperatures can still be generated without reverse breakdown occurring [8], Several researchers have conducted experimental and modeling studies on the reverse bias characteristics of cells [5,15,32]. However, there are few studies that specifically explain the specific impact of reverse bias voltage on abnormal heating of cells under shading conditions.

This study utilized the semiconductor module and heat transfer module in the COMSOL Multiphysics simulation software to establish a finite element model of individual solar cells. The model considered the reverse bias current and local shading, focusing on the semiconductor mechanism of solar cells. Subsequently, this model was combined with experimental data to elucidate the mechanisms underlying temperature abnormalities.

This research contributes to further research on the temperature anomalies of solar cells under partial shading conditions and the development of corresponding mitigation strategies. This research approach can be used to explore the relationship between reverse bias voltage and temperature in photovoltaic modules in actual applications, and to suppress excessively high temperatures through methods that prevent excessive reverse bias voltage.

2. Modeling

The working principle of a monocrystalline silicon cell is based on a p-n junction diode, as shown in Fig. 1. After the formation of the p-n junction, incident light generates excess electron-hole pairs in the diode. The excess electrons and holes diffuse towards the central space charge region and are separated by the built-in electric field present in the space charge region. The photogenerated electron-hole pairs recombine with each other at a finite rate [11].

COMSOL Multiphysics is a versatile simulation software for engineering, manufacturing, and research. The software provides tools for simulating a single physical field, flexibly coupling multiple physical fields, as well as simulation App development and model management. In order to simulate the operating temperature of the solar cell, a model of the solar cell was created in COMSOL Multiphysics. Create the geometry required for each simulation and define the material properties based on the values in the COMSOL material library and literature.

2.1. The process of semiconductor modeling

The semiconductor modeling process referenced the one-dimensional silicon cell modeling process [22] and established a three-dimensional silicon cell model based on it. The p-n junction is formed by p-doping on the surface of the n-type silicon wafer.

The integral expression for the photocarrier generation rate can be written as:

$$G(z) = \int_0^\infty \alpha(\lambda)\phi(\lambda)\exp(-\alpha(\lambda)z)d\lambda \tag{1}$$

where z represents the depth measured from the surface, λ is the wavelength, and $\alpha(\lambda)$ is the absorption coefficient defined by the following expression:

$$\alpha(\lambda) = 4\pi\kappa(\lambda)/\lambda \tag{2}$$

where $\kappa(\lambda)$ is the imaginary part of the refractive index and $\phi(\lambda)$ is the photon generation rate, defined as:

$$\phi(\lambda) = (\lambda/hc) \times F(\lambda) \tag{3}$$

where $F(\lambda)$ represents the spectral irradiance, h is the Planck constant, c is the speed of light. When studying shading conditions, the photogeneration rate in the shaded area is set to zero.

The solution to the coupled Poisson equation and current continuity equation is provided in the semiconductor module:

$$\nabla\cdot(-\varepsilon_0\varepsilon_r\nabla V) = \rho \tag{4}$$

where ε_0 represents the vacuum permittivity, ε_r is the relative permittivity, ρ is the charge density, and V is the potential [24].

Electron and hole composite model choose Shockley-Read-Hall composite model. Analytical doping of N-type is used in the model, geometric doping of P-type is used on the lower surface, and the junction depth is 0.25 μm.

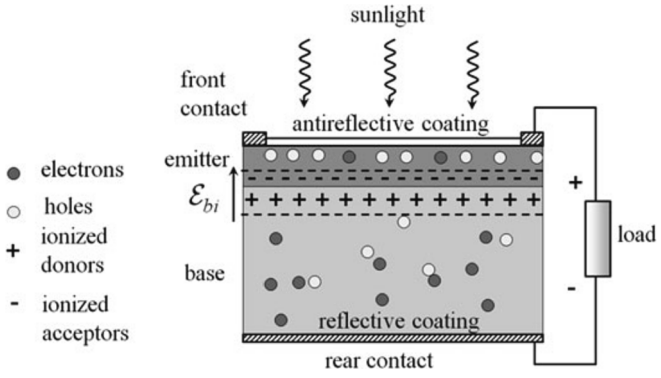

Fig. 1. Solar cell structure [11].

2.2. Temperature modeling

There are two main impacts of shading on the hotspot temperature: (1) an increase in the shaded area causes the shaded cells to further enter reverse bias, resulting in a larger reverse bias voltage across the cell terminals; (2) an increase in the shaded area reduces the illuminated area, leading to a decrease in cell current and the size of the hotspot. These two effects are negatively correlated and together influence the development of the maximum hotspot temperature under partial shading conditions [12].

Based on the main causes of temperature variation due to shading, a thermal model is incorporated into the semiconductor model, assuming convective heat exchange between the upper and lower surfaces of the solar cell and the air, radiative heat transfer between the surface and the environment, and internal heat conduction, as shown in Fig. 2. This can be represented by the following equations [10]:

$$Q_t = Q_{conv} + Q_{rad} + Q_{\Delta T} \tag{5}$$

where Q_t is the total energy of incident solar radiation. Assuming that the upper and lower surfaces of the cell are under natural convection heat transfer conditions, Q_{conv} represents the heat loss due to convective heat transfer with the surrounding atmosphere.

$$Q_{conv} = h\cdot(T - T_{amb})\cdot A \tag{6}$$

where h is the heat transfer coefficient, T is the temperature of cell, T_{amb} is the temperature of surrounding air, and A is the surface area of the cell.

Q_{rad} is the thermal radiation back to the surrounding air and is described as:

$$Q_{rad} = \varepsilon\sigma\left(T^4 - T_{amb}^4\right)A \tag{7}$$

where ε is the surface emissivity and σ is the Stefan-Boltzmann constant.

$Q_{\Delta T}$ represents the heat generated by solar energy cells as they absorb solar energy and use it to heat up. And Heat is transferred through conduction within the solar energy cells.

The main heat sources in the model come from solar radiation and the Joule heat and non-radiative recombination heating of the semiconductor. The heat brought by solar radiation to the cell is generally calculated based on the irradiance and the absorption coefficient of the silicon cell. Considering an irradiance intensity of 1000 W/mˆ2 at AM 1.5, and a silicon material absorption efficiency of approximately 0.8 for solar radiation, the boundary heat source in the model is set to 800 W/mˆ2.

The heat effect of the semiconductor model is added as a generalized heat source to the temperature model. Joule heat refers to the power provided by the electric field per unit volume in the conducting medium, which is consumed as heat in the resistor of the conducting medium. The formula can be written as:

$$Q_J = J\cdot E \tag{8}$$

where J is the current density vector and E is the electric field intensity vector. Specifically, J primarily represents the movement of charge carriers, while E is influenced by the voltage across the terminals of the solar cell.

Non-radiative recombination refers to the recombination of energy in ways other than through radiative photons. The calculation formula for non-radiative recombination is:

$$Q_R = 0.5 \times (\mathrm{e} \times \mathrm{Eg} + 3\mathrm{kT}_I) \times \left(\mathrm{U}_n + \mathrm{U}_p\right) \tag{9}$$

where e represents elementary charge, Eg represents energy gap, k represents Boltzmann constant, T_I represents lattice temperature, U_n represents electron recombination rate, and U_p represents hole recombination rate. The carrier recombination model adopts the Shockley-Read-Hall (SRH) model, where the recombination rates for electrons and holes are assumed to be equal, expressed as:

$$U_n = U_p = \left(np - n_i^2\right)/\left(\tau_n(p + p_1) + \tau_p(n + n_1)\right) \tag{10}$$

where n and p represent the concentrations of electrons and holes, n_i is the square root of the product of the electron and hole concentrations at equilibrium., τ_n and τ_p are the lifetimes of electrons and holes respectively, and n_1 and p_1 represent the additional carrier concentrations caused by surface states.

In order to simplify the model, assuming the area of the solar cell is completely shaded with no irradiation.

2.3. Geometry and materials

In order to facilitate subsequent design experiments, the geometric dimensions of the silicon wafer in the model are 158 mm × 39.5 mm, with a thickness of 150 μm. When partitioning the grid, refining the model grid in the thickness direction is beneficial for the calculation of semiconductor models, as shown in Fig. 3. The material chosen is silicon from the material library provided by the COMSOL Multiphysics, and the material properties are shown in Table 1 [6]. The solar irradiance spectrum and the silicon absorption spectrum are given as shown in Fig. 4 and Fig. 5.

3. Experiment

This experiment uses a solar cell module consisting of six solar cells connected in series as the research object. The I-V curve and P-V curve of a single cell are shown in Fig. 6, with dimensions of 158 mm × 39.5 mm. Measuring the electrical parameters of shaded and unshaded cells in the module., as shown in Fig. 7. An external electronic load is connected to the solar cell module to control its output. The electronic load is set to

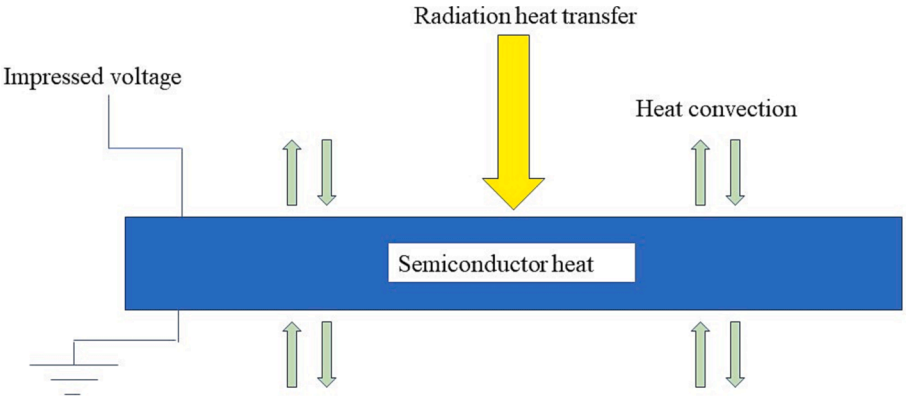

Fig. 2. Illustration of heat transfer in a silicon solar cell.

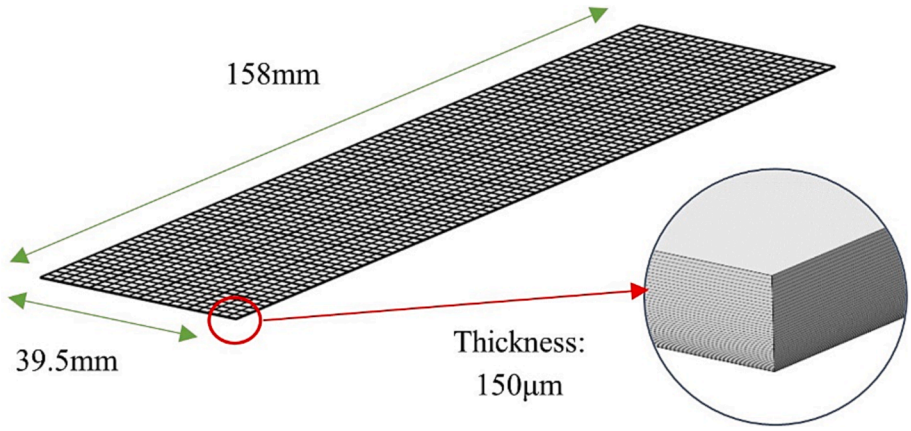

Fig. 3. Geometry and meshing.

Table 1
Material properties.

symbol	property	value	unit
ε_r	relative dielectric constant	11.7	1
h	heat conductivity coefficient	131	W/(m • K)
ρ	density	2329	kg/mˆ3
C_p	heat capacity at constant pressure	700	J/(kg • K)
τ_n	Electron lifetime	10	us
τ_p	Hole lifetime	10	us
Eg	band gap	1.12	V
μ_n	electronic mobility	1450	cmˆ2/(V • s)
μ_p	hole mobility	500	cmˆ2/(V • s)
ε	surface emissivity	0.8	1

operate in a constant current mode of 2A, enabling the cells to operate near their maximum power point. When the photocurrent generated by the solar cell module is less than 2A, the electronic load no longer acts as a limiting current, but rather functions as a small resistor in the circuit. For the experiment, a xenon lamp is used as the light source to simulate solar irradiation, with an irradiance of 1000 W/mˆ2. The temperature of the solar cell module is measured using a thermal imaging camera [27], and real-time irradiance is measured using an irradiance meter, as shown in Fig. 8.

During the experiment, an opaque shield is used to cover the surface of the solar cell, achieving the effect of shading. The shading direction starts from the short side and gradually increases the shading range along the long side.

4. Results and discussion

4.1. Experimental result

Thermal images of the solar cell were captured during the experiment with different shading areas, as shown in Fig. 9. Cell data was recorded after shading different areas and plotted on a chart. The shading areas were normalized for analysis. In the experiment, the temperature of the shaded cells changed with the variation in shading area, while the temperature of the unshaded cells remained consistently

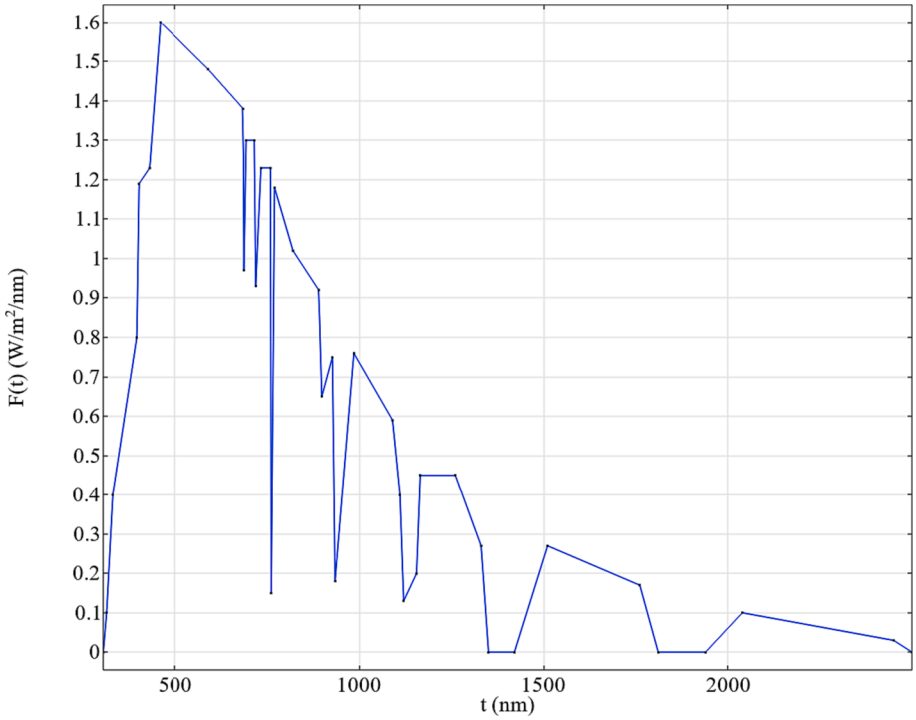

Fig. 4. Solar spectrum [6].

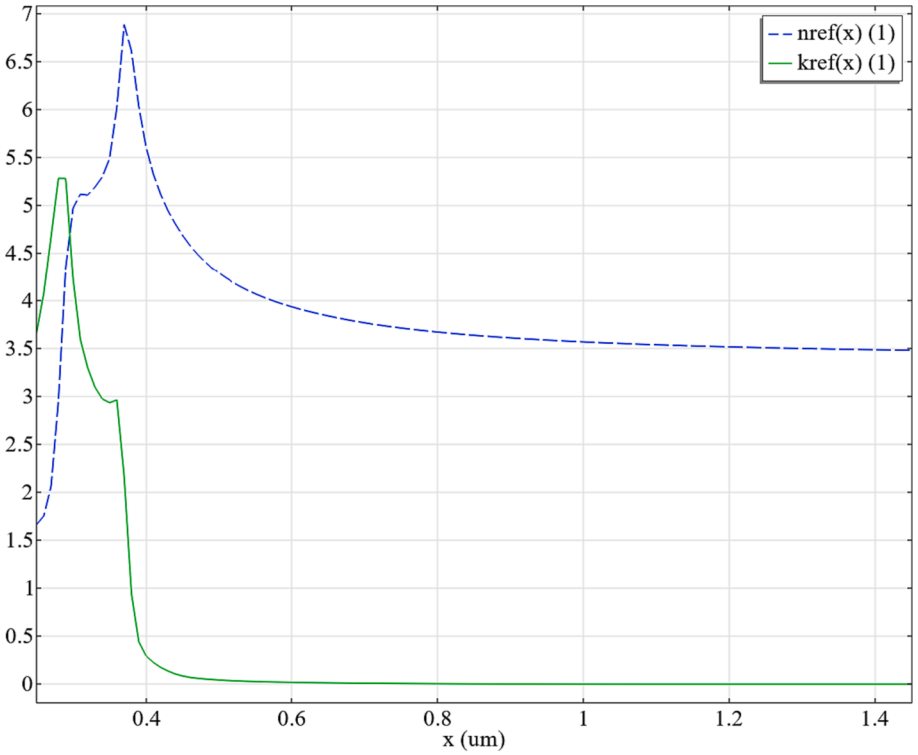

Fig. 5. Silicon absorption spectrum [6].

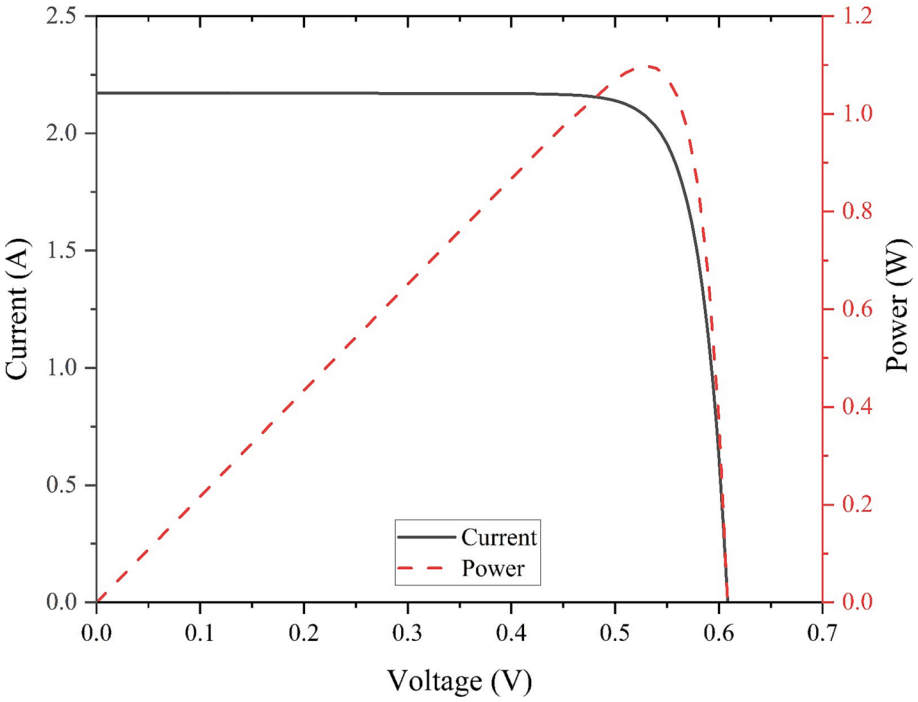

Fig. 6. Test cell performance.

around 76 °C. The temperature obtained by the test is given in the Table 2.

From Fig. 10, it can be observed that when the shading area is small (shade area less than 10 %), the voltage of the shaded cell remains relatively constant compared to the control group. This is because shading mainly affects the short-circuit current of the cell's I-V curve, while having a minimal impact on the voltage. As the shading area increases, the short-circuit current of the cell decreases significantly.

In the experiment, a constant current mode of 2A was used for the electronic load. When the short-circuit current of the shaded cell is greater than the set operating current, the cell can still operate at a forward bias voltage, but with a slight difference in voltage compared to the other unshaded cells. When the shading reaches a certain degree, approximately 25 % of the total area, the short-circuit current of the

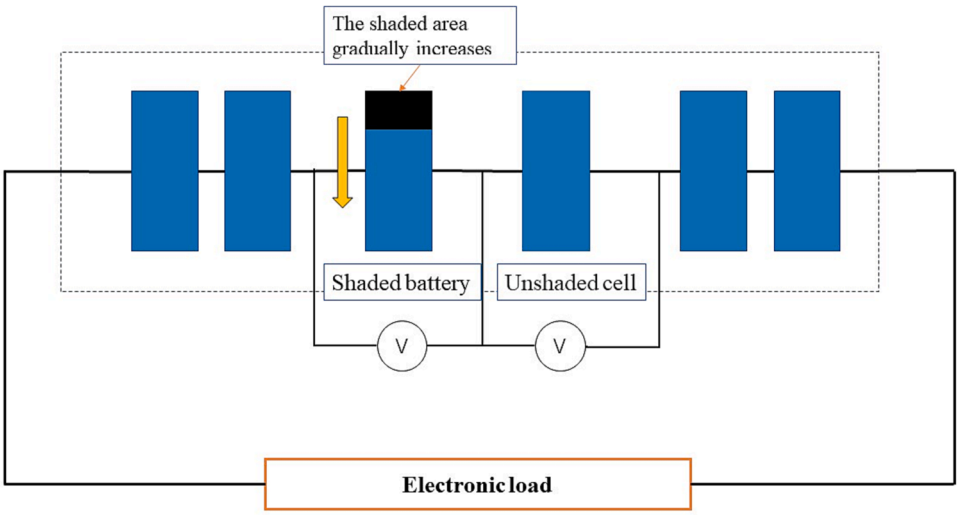

Fig. 7. Experimental design diagram.

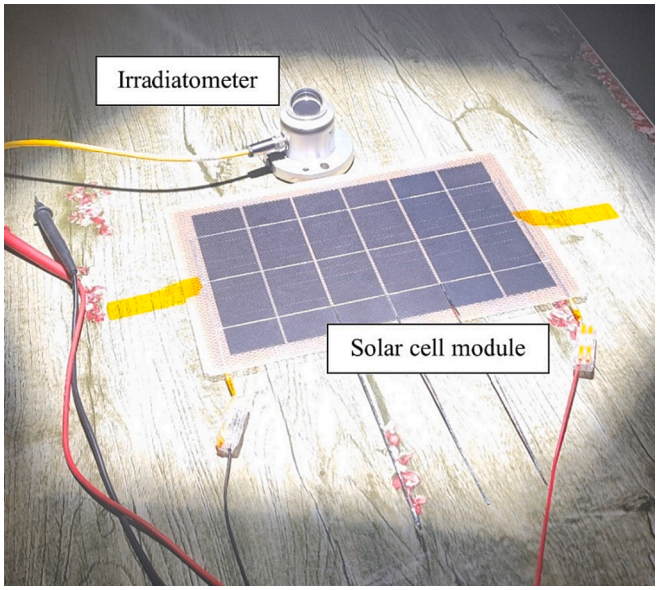

Fig. 8. The solar cell module used for the experiment.

shaded cell is insufficient to support the operating current. At this point, a reverse bias voltage quickly develops across the terminals of the shaded cell, causing the voltage of the electronic load to rapidly decrease. When the shading area reaches 37.5 %, the voltage of the external circuit drops to 0.23 V, while the reverse bias voltage of the shaded cell reaches 2.13 V, as shown in Fig. 11.

At this point, the output power of the solar cell module quickly decreases, with shaded cells acting as a load and consuming the output power of other normal cells, accompanied by a rapid increase in temperature. With the increase of the shading area, the voltage of the external circuit further decreases, approaching 0, while the voltage of the unshaded cells gradually increases, approaching the open circuit voltage. The shaded cell, acting as a load, reaches a reverse bias voltage of 2.83 V, which is equivalent to the sum of the voltages of the remaining unshaded cells.

From Fig. 12, it can be observed that when the shaded cell reaches around 25 %, it transitions into a load that consumes a large amount of power, peaking at 4 W. The power consumption of the external load decreases significantly. As the shading area increases further, the output power of the unshaded cell gradually decreases, and the power consumption of the shaded cell also decreases. This is also the reason for the decrease in temperature of the shaded cell as shown in Fig. 11. This is because the variation in current in the circuit causes the operating voltage of the unshaded cell to approach the open-circuit voltage, deviating from the maximum power point at around 0.51 V. The output power continuously decreases, eventually causing the entire circuit to approach an open-circuit state with extremely low output power, as

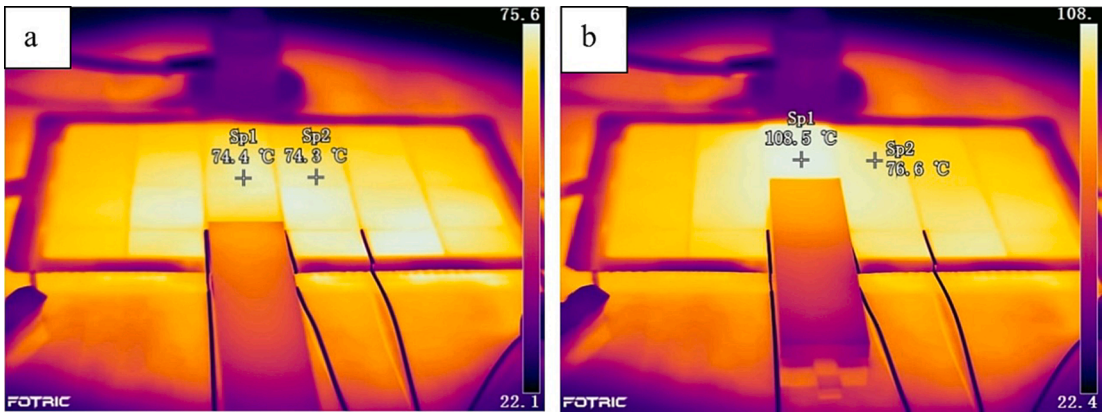

Fig. 9. Thermal image, (a) shading range 12.5%; (b) shading range 50%.

Table 2
Temperature data of shaded cell obtained by test.

Shading range (%)	0	12.5	18.75	25	28.125	31.25	37.5
Temperature (℃)	75	76	76.5	76.5	76	94.2	107.7
Shading range (%)	43.75	50	62.5	75	87.5	93.75	/
Temperature (℃)	108.9	108.6	108.5	104.7	92.4	83	/

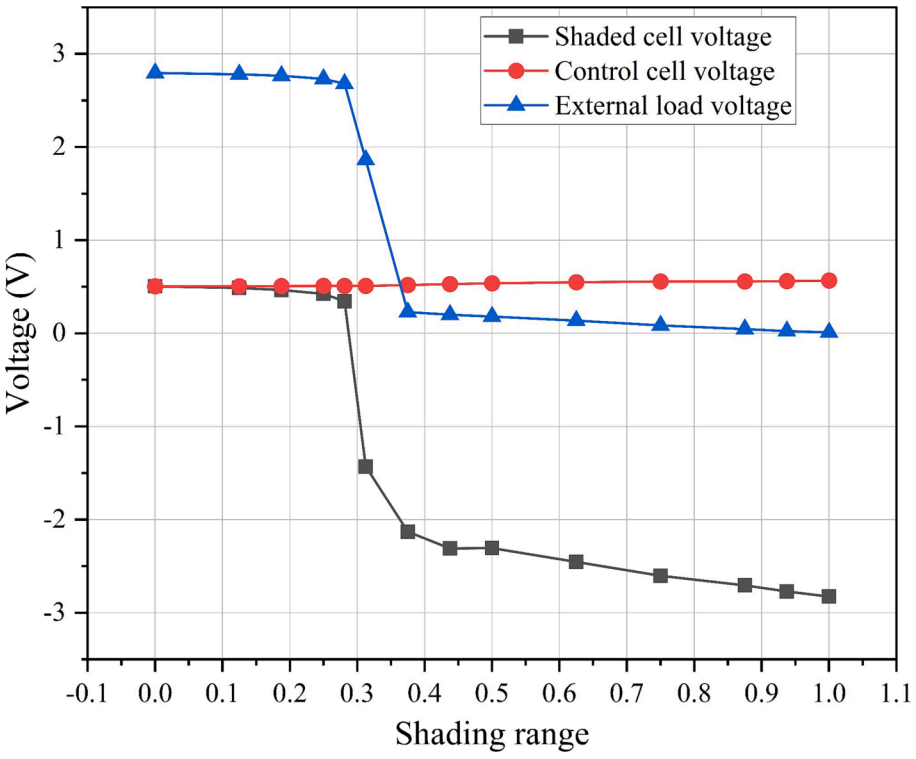

Fig. 10. Effect of shading range of single solar cell on output voltage.

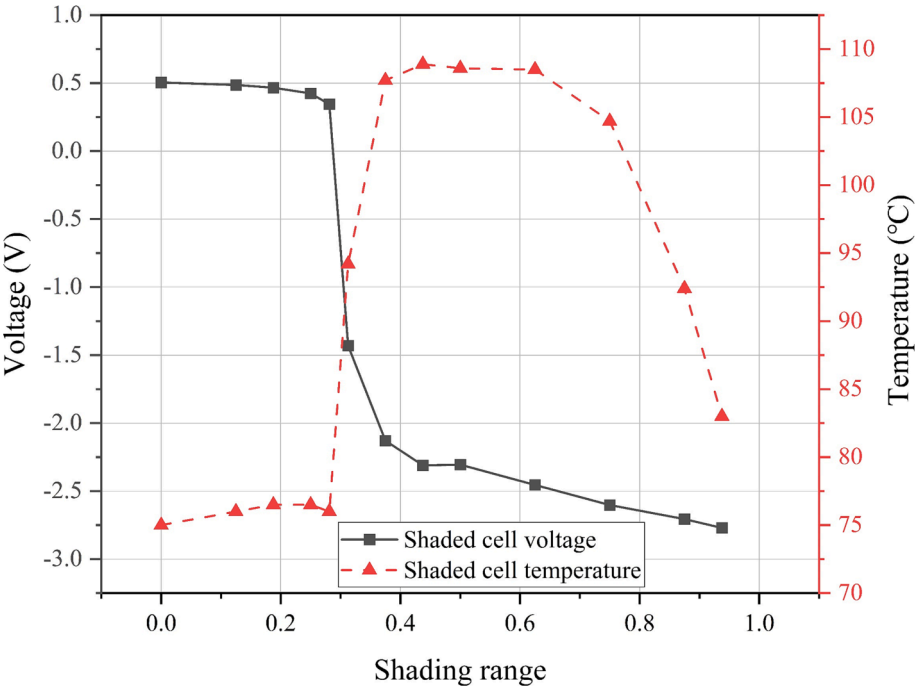

Fig. 11. The relationship between shaded cell voltage and temperature with shading range.

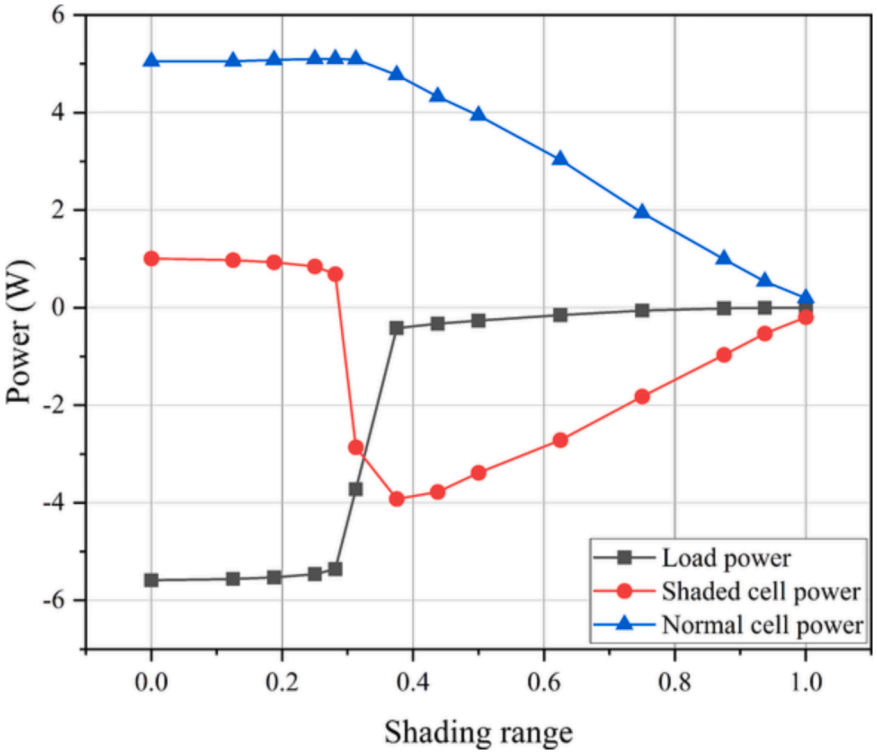

Fig. 12. Variation of power with changes in the shaded area.

shown in Fig. 13.

4.2. Simulation result discussion

The environmental conditions set in the simulation match the experimental conditions. The ambient temperature is set at 35 °C, and the natural convection heat transfer coefficient is empirically set at 5 W/(mˆ2·K). The voltage at the terminal of the shaded cells under different shading areas, obtained from the experiment, is input into the model to obtain the simulated temperature distribution of the cells under different shading areas. The simulated temperature image obtained is shown in Fig. 14. Fig. 15 compares the experimental and simulated temperatures. Based on the observed similar trends in both simulated and experimental data, as well as an average relative deviation of 0.9 % and a maximum relative deviation of 8.1 % between the two data sets, it can be concluded that the simulation model has been validated by the

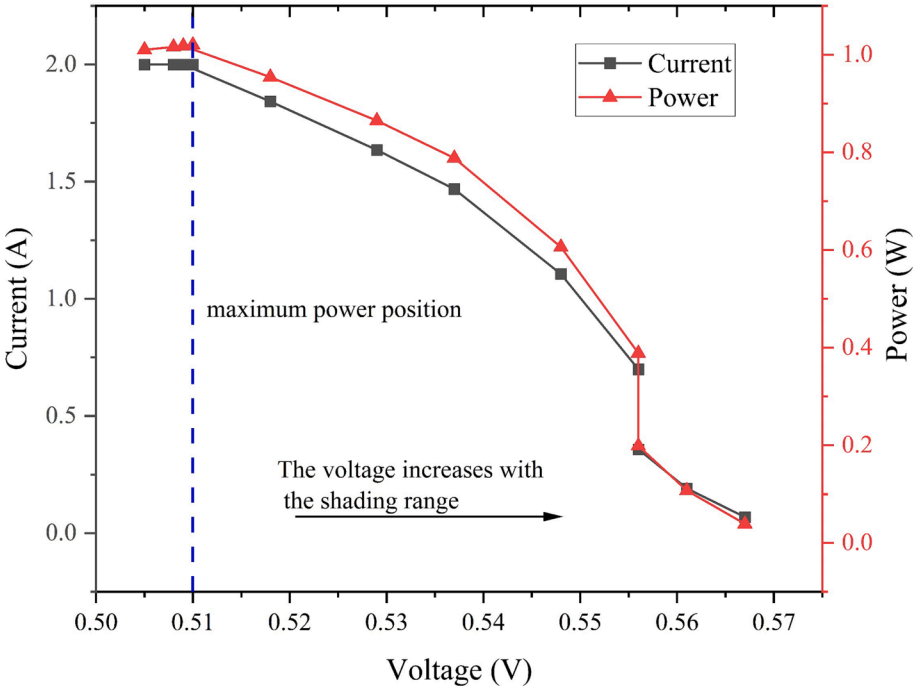

Fig. 13. Changes in electrical parameters of unshaded cell.

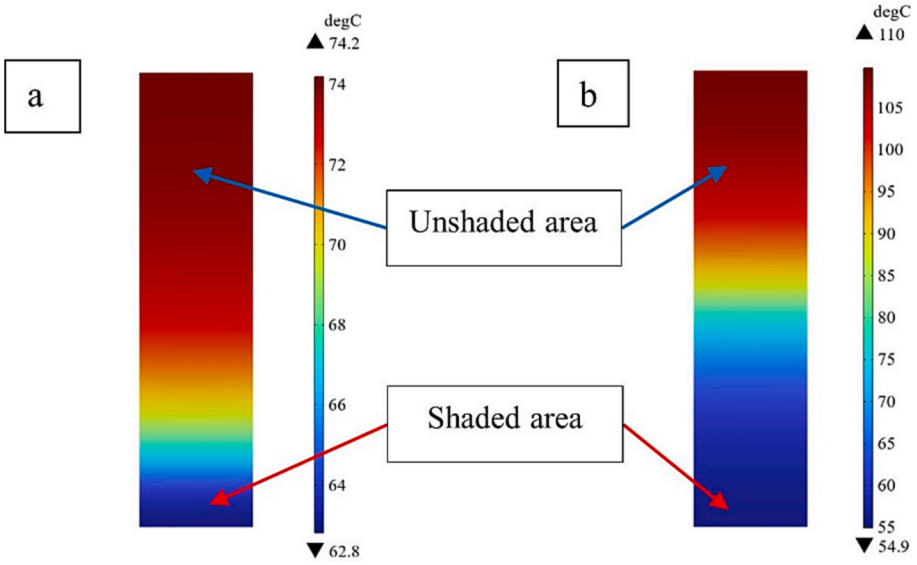

Fig. 14. Temperature simulation, (a) shading range 12.5%; (b) shading range 50%.

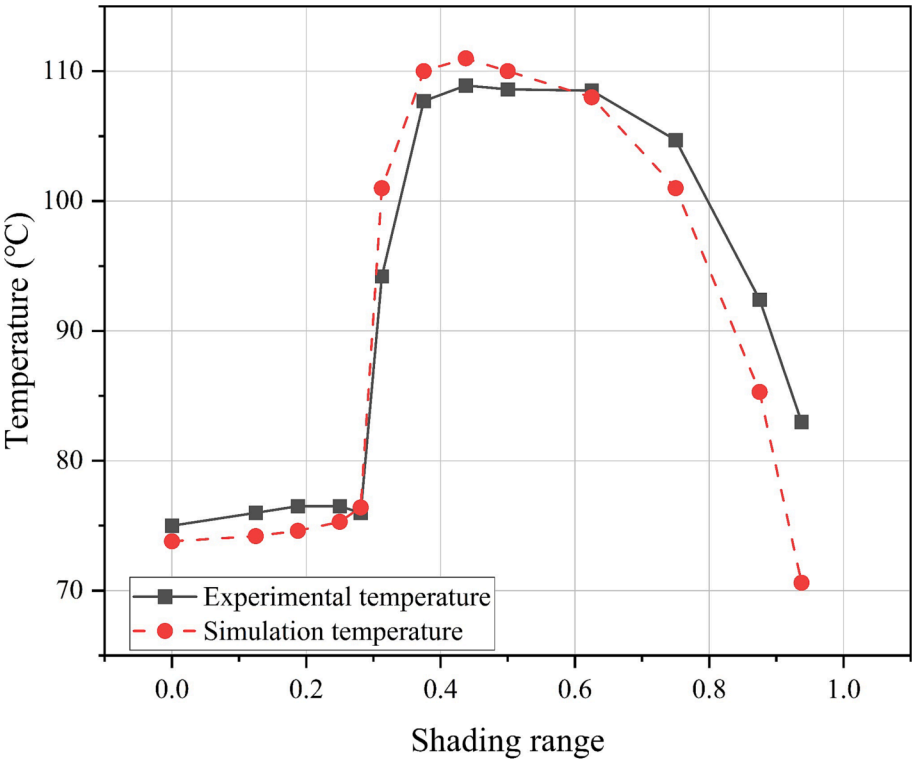

Fig. 15. Comparing the simulated and experimental high-temperature region temperatures of the shaded cell.

experiments.

Fig. 16 illustrates the variation of the main heat sources in the simulation under different shading ratios, where the heat flow is composed of convective heat transfer and radiative heat transfer. It can be observed that the heat flow changes in a decreasing trend, even reaching negative values. This is because as the shaded area increases, the radiative heat transfer flux decreases proportionally until the inward radiative heat transfer flux becomes smaller than the outward convective heat transfer flux. As a result, the total heat flow transitions from increasing the cell temperature to heat dissipation. The non-radiative recombination heat remains negative, indicating heat absorption. This is because carrier recombination requires photon energy, and as the shielding area increases, the radiative area decreases, resulting in a decrease in photon energy and the corresponding decrease in the energy available to support carrier recombination, resulting in a uniform decrease in the non-radiative recombination heat. The Joule heat component is related to the reverse bias voltage. When the voltage at both ends of the cell is reversed, the Joule heat increases sharply, reaching a peak value of 3.73 W. As the shielding range further increases, the Joule heat begins to decrease, consistent with the temperature change trend. This is mainly related to the current density, electric field intensity, and the area of the irradiation region.

The distribution of solar cell current density under different shading areas can be observed in the simulation model, as shown in Fig. 17. As

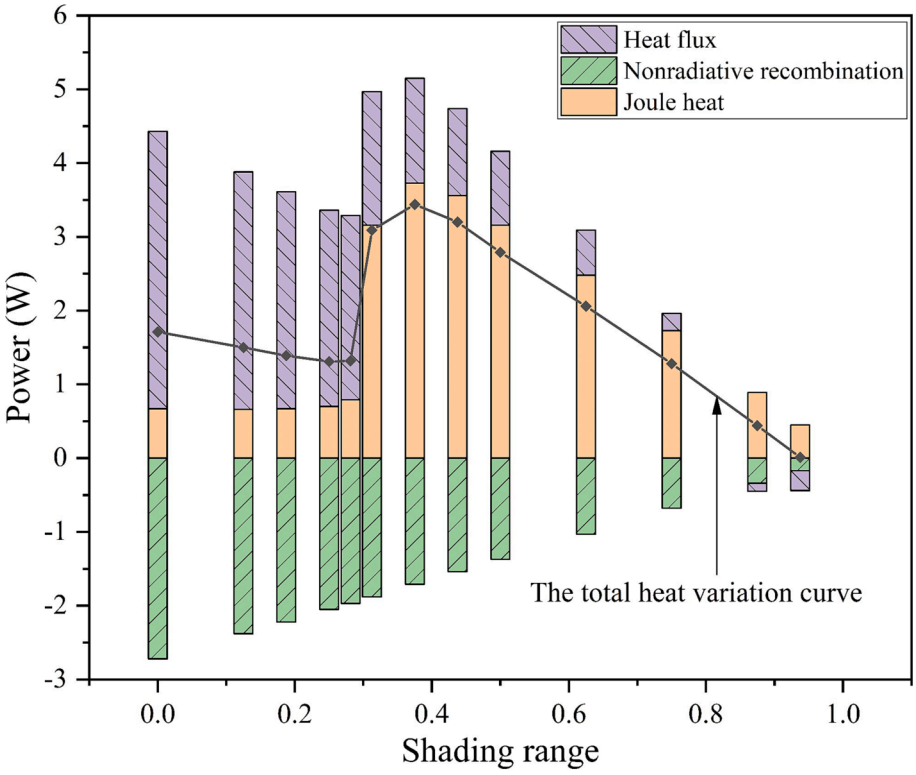

Fig. 16. Variation of the main heat source with changes in the shaded area.

shown in Fig. 18, during the process of increasing the reverse voltage at the ends of the shaded cell, the current density in the unshaded region exhibits a trend of decreasing with the decrease of the positive voltage and increasing with the positive voltage. However, in the absence of breakdown in the semiconductor, the upper limit of the current density is determined by the density of electrons and holes in the semiconductor, which, according to the model, is calculated to be 317 (A/m^2) in our study. After reaching the upper limit of the current density, increasing the reverse voltage will not further increase the current density. The current density in the shaded part is relatively small compared to the unshaded part, and it is in the opposite direction. It gradually decreases as the reverse voltage increases, until it approaches zero.

The distribution of electric field intensity in the cell is influenced by terminal voltage, while solar cells mainly rely on charge carriers to create an electric field. The impact of different shading areas on the distribution of the electric field is mainly reflected near the p-n junction. Fig. 19 shows the variation of electric field intensity near the p-n junction with thickness. The distribution of electric field away from the p-n

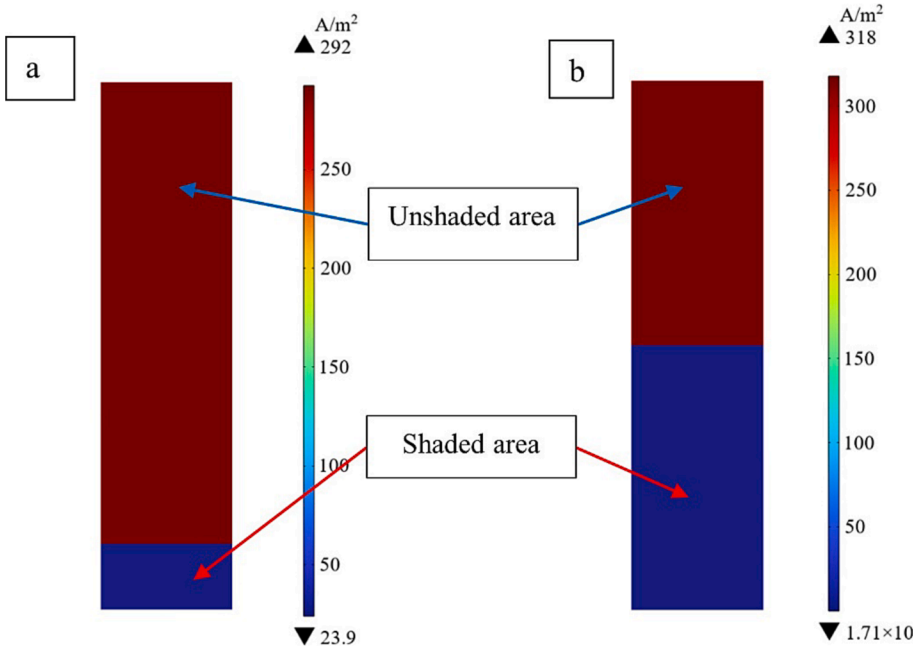

Fig. 17. Current density simulation, (a) shading range 12.5%; (b) shading range 50%.

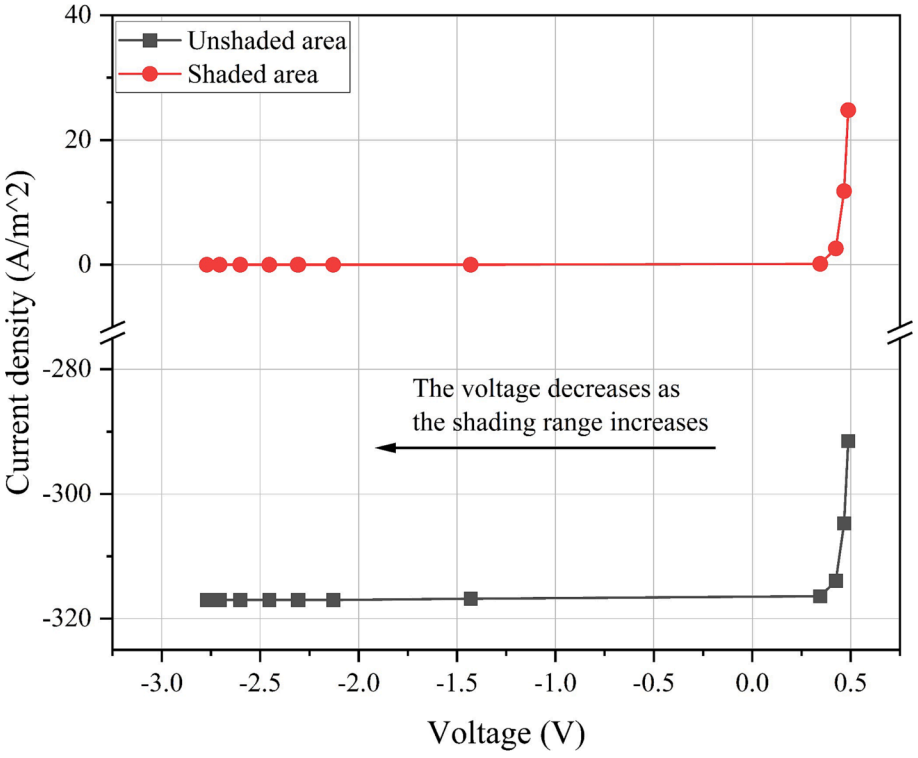

Fig. 18. Variation of current density.

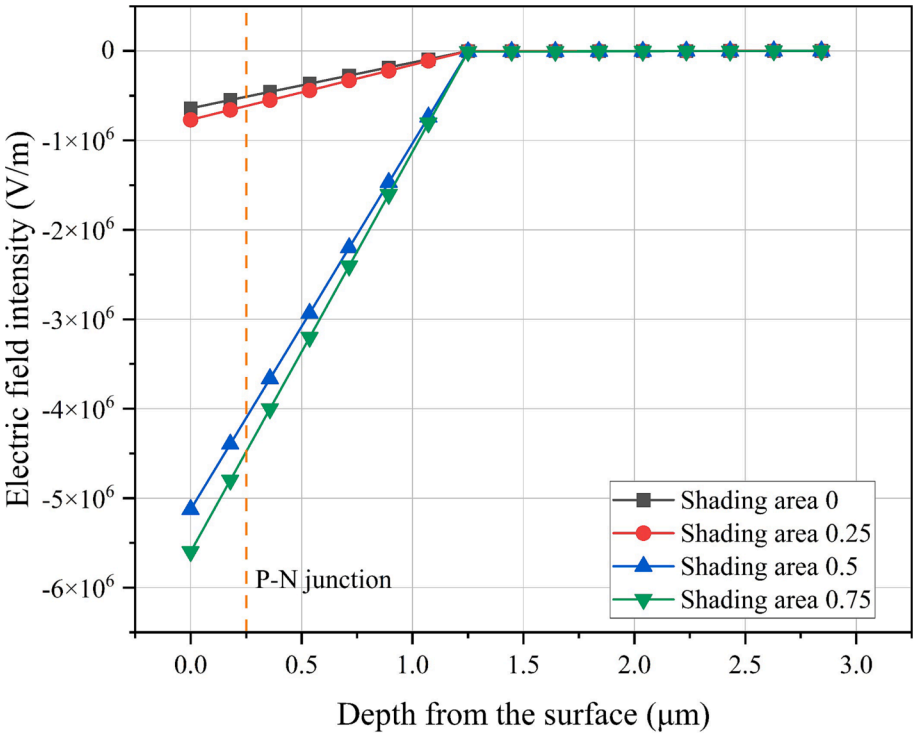

Fig. 19. Electric field intensity distribution.

junction is generally consistent.

According to the calculation method of Joule heating, the variation of Joule heat per unit volume can be determined with the change in irradiation range, as shown in Fig. 20.

5. Conclusion

This article investigates the temperature anomalies that occur in individual cells of a series-connected cell module operating at lower voltages when shaded, and analyzes the causes of these anomalies by experimental and multi-physics field coupled model simulation.

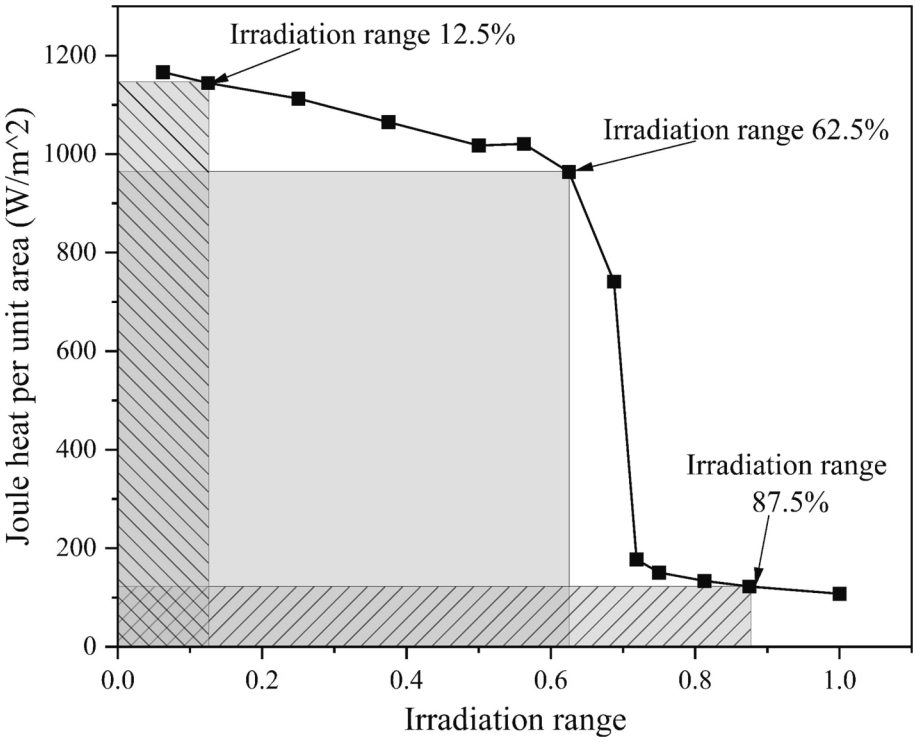

Fig. 20. Irradiation range Joule heat per unit area, the shaded area represents the total Joule heating generated by different irradiation range.

From experimental and simulation results, it can be observed that the shading range of 40 % to 60 % has the greatest impact on the temperature of solar cell. Joule heating is the primary cause of drastic temperature changes, and it is influenced by current density and electric field intensity. The highest temperature produced by a cell due to shading, without being punctured, depends on the maximum current density allowed by the cell and the voltage provided by other unshaded cells. Shading has a negative impact on the short-circuit current of solar cells. However, if the shaded cells can still meet the current requirements for normal operation of the circuit, although the power of the shaded cells is reduced, they still operate within the positive bias voltage range. This is why there is no significant temperature increase observed in experiments with small-area shading (around 10 %). In the case of extensive shadowing (covering more than 80 % of the surface), the current density in the shaded portion of the cell is extremely low, resulting in minimal Joule heating. Even if the reverse bias voltage is increased, it cannot compensate for the heat loss in this shaded area. Therefore, the cell may experience a decrease in temperature instead.

Our next step is to conduct research on partial shading with multiple cells and attempt to scale up the component size to test and refine the simulation methods proposed in this study. Additionally, through this approach, we may investigate how to judiciously select the number and placement of bypass diodes in series-connected components to prevent excessively high reverse bias voltages, achieving the goal of suppressing excessive temperature.

Declaration of competing interest

The authors declare that they have no known competing financial interests or personal relationships that could have appeared to influence the work reported in this paper.

Acknowledgements

This work was supported by the National Natural Science Foundation of China [grant numbers 51775021], the Fundamental Research Funds for the Central Universities [grant numbers YWF-23-JC-02, YWF-23-JC-09]

References

[1] A. Al Tarabsheh, M. Akmal, M. Ghazal, Series Connected Photovoltaic Cells—Modelling and Analysis, Sustainability 9 (2017) 371, https://doi.org/10.3390/su9030371.
[2] J. Bai, Y. Cao, Y. Hao, Z. Zhang, S. Liu, F. Cao, Characteristic output of PV systems under partial shading or mismatch conditions, Solar Energy 112 (2015) 41–54, https://doi.org/10.1016/j.solener.2014.09.048.
[3] C. Breyer, D. Bogdanov, A. Aghahosseini, A. Gulagi, M. Child, A.S. Oyewo, J. Farfan, K. Sadovskaia, P. Vainikka, Solar photovoltaics demand for the global energy transition in the power sector, Progress in Photovoltaics: Research and Applications 26 (2018) 505–523, https://doi.org/10.1002/pip.2950.
[4] C.E. Clement, J.P. Singh, E. Birgersson, Y. Wang, Y.S. Khoo, Hotspot development and shading response of shingled PV modules, Solar Energy 207 (2020) 729–735, https://doi.org/10.1016/j.solener.2020.06.078.
[5] A. Compagnin, M. Meneghini, M. Barbato, V. Giliberto, A. Cester, M. Vanzi, G. Mura, E. Zanoni, G. Meneghesso, Thermal and electrical investigation of the reverse bias degradation of silicon solar cells, Microelectronics Reliability, European Symposium on Reliability of Electron Devices, Failure Physics and Analysis 53 (2013) 1809–1813, https://doi.org/10.1016/j.microrel.2013.07.013.
[6] COMSOL Multiphysics® v. 6.0, 2021. models.semicond.si_solar_cell_1d.
[7] S. Daliento, F. Di Napoli, P. Guerriero, V. d'Alessandro, A modified bypass circuit for improved hot spot reliability of solar panels subject to partial shading, Solar Energy 134 (2016) 211–218, https://doi.org/10.1016/j.solener.2016.05.001.
[8] Danner, M., Bucher, K., 1997. Reverse characteristics of commercial silicon solar cells-impact on hot spot temperatures and module integrity, in: Conference Record of the Twenty Sixth IEEE Photovoltaic Specialists Conference - 1997. Presented at the Conference Record of the Twenty Sixth IEEE Photovoltaic Specialists Conference - 1997, IEEE, Anaheim, CA, USA, pp. 1137–1140. https://doi.org/10.1109/PVSC.1997.654289.
[9] A. Dolara, G.C. Lazaroiu, S. Leva, G. Manzolini, Experimental investigation of partial shading scenarios on PV (photovoltaic) modules, Energy 55 (2013) 466–475, https://doi.org/10.1016/j.energy.2013.04.009.
[10] Y. Du, W. Tao, Y. Liu, J. Jiang, H. Huang, Heat transfer modeling and temperature experiments of crystalline silicon photovoltaic modules, Solar Energy 146 (2017) 257–263, https://doi.org/10.1016/j.solener.2017.02.049.
[11] M. Evstigneev, Introduction to Semiconductor Physics and Devices, Springer International Publishing, Cham. (2022), https://doi.org/10.1007/978-3-031-08458-4.
[12] I. Geisemeyer, F. Fertig, W. Warta, S. Rein, M.C. Schubert, Prediction of silicon PV module temperature for hot spots and worst case partial shading situations using spatially resolved lock-in thermography, Solar Energy Materials and Solar Cells 120 (2014) 259–269, https://doi.org/10.1016/j.solmat.2013.09.016.

[13] D. Giaffreda, M. Omaña, D. Rossi, C. Metra, Model for Thermal Behavior of Shaded Photovoltaic Cells under Hot-Spot Condition, in: In: 2011 IEEE International Symposium on Defect and Fault Tolerance in VLSI and Nanotechnology Systems. Presented at the 2011 IEEE International Symposium on Defect and Fault Tolerance in VLSI and Nanotechnology Systems (DFT), 2011, pp. 252–258, https://doi.org/10.1109/DFT.2011.47.
[14] Herrmann, W., Wiesner, W., Vaassen, W., 1997. Hot spot investigations on PV modules-new concepts for a test standard and consequences for module design with respect to bypass diodes, in: Conference Record of the Twenty Sixth IEEE Photovoltaic Specialists Conference - 1997. Presented at the Conference Record of the Twenty Sixth IEEE Photovoltaic Specialists Conference - 1997, pp. 1129–1132. https://doi.org/10.1109/PVSC.1997.654287.
[15] Jin, Y., Ikeda, K., Doi, T., 2011. Reverse bias test of c-Si single-cell PV modules, in: Reliability of Photovoltaic Cells, Modules, Components, and Systems IV. Presented at the Reliability of Photovoltaic Cells, Modules, Components, and Systems IV, SPIE, pp. 251–259. https://doi.org/10.1117/12.893407.
[16] A.K. Kadhim, M.R. Mohammad, A.I. Abd Ali, M.K.A. Mohammed, Reduced Graphene Oxide/Bi2O3 Composite as a Desirable Candidate to Modify the Electron Transport Layer of Mesoscopic Perovskite Solar Cells, Energy Fuels 35 (2021) 8944–8952, https://doi.org/10.1021/acs.energyfuels.1c00848.
[17] O. Kunz, R.J. Evans, M.K. Juhl, T. Trupke, Understanding partial shading effects in shingled PV modules, Solar Energy 202 (2020) 420–428, https://doi.org/10.1016/j.solener.2020.03.032.
[18] R.S. Magdaleno, P.A. Sánchez-Pérez, J.L.Z. Ramírez Cruz, D.M. Escobar, A. Sánchez-Juárez, Influence of partial shading on the power output of a solar cell and a PV module, in: In: 2018 IEEE 7th World Conference on Photovoltaic Energy Conversion (WCPEC) (a Joint Conference of 45th IEEE PVSC, 28th PVSEC & 34th EU PVSEC). Presented at the 2018 IEEE 7th World Conference on Photovoltaic Energy Conversion (WCPEC) (a Joint Conference of 45th IEEE PVSC, 28th PVSEC & 34th EU PVSEC), 2018, pp. 1324–1327, https://doi.org/10.1109/PVSC.2018.8547680.
[19] M.R. Maghami, H. Hizam, C. Gomes, M.A. Radzi, M.I. Rezadad, S. Hajighorbani, Power loss due to soiling on solar panel: A review, Renewable and Sustainable Energy Reviews 59 (2016) 1307–1316, https://doi.org/10.1016/j.rser.2016.01.044.
[20] P. Mertia, S. Kothari, N. Agrawal, N.L. Panwar, Experimental Analysis of Solar Photovoltaic System under Partial Shading, Int. J. Curr. Microbiol. App. Sci 9 (2020) 1623–1630. https://doi.org/10.20546/ijcmas.2020.910.194.
[21] H. Mohammed, M. Kumar, R. Gupta, Bypass diode effect on temperature distribution in crystalline silicon photovoltaic module under partial shading, Solar Energy 208 (2020) 182–194, https://doi.org/10.1016/j.solener.2020.07.087.
[22] J. Nayak, D.K. Mishra, P. Pattanaik, Numerical modelling and simulation of a 1-D Silicon solar cell, Materials Today: Proceedings 41 (2021) 451–454, https://doi.org/10.1016/j.matpr.2020.10.233.
[23] I.H. Rusiana, Z.Y. Bakti, S. Sambasri, Study and Analysis of Shading Effects on Photovoltaic Application System, MATEC Web Conf. 218 (2018) 02004, https://doi.org/10.1051/matecconf/201821802004.
[24] P. Saxena, N.E. Gorji, COMSOL Simulation of Heat Distribution in Perovskite Solar Cells: Coupled Optical–Electrical–Thermal 3-D Analysis, IEEE JOURNAL OF PHOTOVOLTAICS 9 (2019) 6.
[25] T. Sebbagh, R. Kelaiaia, A. Zaatri, An experimental validation of the effect of partial shade on the I-V characteristic of PV panel, Int J Adv Manuf Technol 96 (2018) 4165–4172, https://doi.org/10.1007/s00170-018-1858-4.
[26] A. Sharma, V. Balaji Venkateswaran, R. Singh, Experimental Analysis of Electrical and Thermal Effects of Various Configurations of Partial Shading on Three Different Solar Module Technologies, in: In: 2018 International Conference on Recent Trends in Electrical, Control and Communication (RTECC). Presented at the 2018 International Conference on Recent Trends in Electrical, Control and Communication (RTECC), 2018, pp. 137–142, https://doi.org/10.1109/RTECC.2018.8625650.
[27] J.A. Tsanakas, L. Ha, C. Buerhop, Faults and infrared thermographic diagnosis in operating c-Si photovoltaic modules: A review of research and future challenges, Renewable and Sustainable Energy Reviews 62 (2016) 695–709, https://doi.org/10.1016/j.rser.2016.04.079.
[28] M. Vumbugwa, F.J. Vorster, J.L.C. McCleland, E.E. van Dyk, Effects of changing partial cell shading on the electrical and thermal characteristics of crystalline silicon photovoltaic module, Solar Energy 240 (2022) 147–156, https://doi.org/10.1016/j.solener.2022.05.031.
[29] C. Wang, L. Huang, Y. Zhou, Y. Guo, K. Liang, T. Wang, X. Liu, J. Zhang, Z. Hu, Y. Zhu, Perovskite Solar Cells in the Shadow: Understanding the Mechanism of Reverse-Bias Behavior toward Suppressed Reverse-Bias Breakdown and Reverse-Bias Induced Degradation, Advanced Energy Materials 13 (2023) 2203596, https://doi.org/10.1002/aenm.202203596.
[30] R. Witteck, S. Blankemeyer, M. Siebert, M. Köntges, H. Schulte-Huxel, Partial shading of one solar cell in a photovoltaic module with 3-terminal cell interconnection, Solar Energy Materials and Solar Cells 219 (2021) 110811, https://doi.org/10.1016/j.solmat.2020.110811.
[31] J. Wu, L. Zhang, Z. Liu, Z. Wu, Coupled optical-electrical-thermal analysis of a semi-transparent photovoltaic glazing façade under building shadow, Applied Energy 292 (2021) 116884, https://doi.org/10.1016/j.apenergy.2021.116884.
[32] A. Zegaoui, P. Petit, M. Aillerie, J.P. Sawicki, A.W. Belarbi, M.D. Krachai, J. P. Charles, Photovoltaic Cell/Panel/Array Characterizations and Modeling Considering Both Reverse and Direct Modes, Energy Procedia, Impact of Integrated Clean Energy on the Future of the Mediterranean Environment? 6 (2011) 695–703, https://doi.org/10.1016/j.egypro.2011.05.079.